



1 **Impact of refreezing melt ponds on Arctic sea ice basal growth**

2 Daniela Flocco (1), Daniel L. Feltham (1), David Schröder (1), Michel Tsamados (2)

3 (1) Centre for Polar Observations and Modelling - Department of Meteorology, University of Reading

4 (2) Centre for Polar Observations and Modelling - Department of Earth Sciences, University College
5 London

6

7 Corresponding author: d.flocco@reading.ac.uk

8



9 **1. Abstract**

10 Melt ponds forming over the sea ice cover in the Arctic profoundly impact the surface albedo inducing
11 a positive feedback leading to further melting.

12 Here we examine the processes involved in melt pond refreezing and their impact on basal sea ice
13 growth.

14 When ponds freeze, the ice that forms on them insulates the pond trapping it between the sea ice and
15 the ice lid. Trapped melt ponds delay basal sea ice growth in Autumn: ice thickens only after (1) the
16 pond water has been fully frozen and (2) a temperature gradient is established that will conduct heat
17 away from the ocean. Sea ice thickening in the areas where ponds are present is mainly due to the
18 pond's water refreezing. Pan-Arctic simulations with a stand-alone sea ice model and studies with a
19 high-resolution one-dimensional, three-layer refreezing model are used to study the impact on sea ice
20 growth of trapped melt ponds. Basal sea ice growth may be inhibited by up to two months. We estimate
21 an inhibited basal growth of up to 228 km³, which represents 25% of the basal sea ice growth estimated
22 by PIOMAS during the months of September and October. The brine not released due to the inhibited
23 basal growth during this period could have implications for the ocean properties and circulation. The
24 impact of trapped melt ponds has not been accounted for so far in any climate model.

25
26
27
28

Key points

- 29 • Melt pond refreezing inhibits basal sea ice growth.
30 • Internal temperature profile is impacted by the presence of refreezing ponds.
31 • CICE results show a total over-estimation of basal sea ice growth in Sept - Oct of up to more
32 than 200 km³.

33



34 **1. Introduction**

35 The decline of Arctic Sea ice in the past 25 years has been observed and discussed extensively. In the
36 mid-1980s multi-year ice (MYI) accounted for 70% of total winter ice extent, whereas by the end of
37 2012, it had dropped to less than 20% [Stroeve et al., 2014].

38 The maintenance of the sea ice system results from a balance of atmosphere - ice-ocean
39 thermodynamic and dynamic processes, and the causes of the observed sea ice reduction are complex
40 [Perovich and Richter-Menge, 2009]. Larger areas of open water observed in the summer increase the
41 heat storage in the ocean, leading to increased water temperatures resulting in additional bottom melt of
42 sea ice [Perovich et al., 2008, Perovich et al., 2009, Tsamados et al, 2015] and a consequent delay in
43 winter sea ice formation.

44 The solar energy input into the ocean is affected both by the high albedo of sea ice compared to
45 seawater (bare sea ice and snow reflectivity can be up to ~85%; that of water is ~10% [Perovich,
46 2009]) and the internal absorption of radiation by sea ice. On these grounds it is straightforward to
47 understand the importance of features such as melt ponds that form during spring from snow and ice
48 melt because they lower the total sea ice albedo by up to 20% [Perovich et al. 2002].

49 Flocco et al. [2012] performed a number of sensitivity studies to evaluate the impact of including melt
50 ponds in the sea ice component of Global Climate Models (GCMs hereafter) showing a decrease of up
51 to 30% in the surface albedo over the summer months and an average decrease in the September sea ice
52 volume of 40%. Schroeder et al. [2014] showed that the observed September sea ice extent can be
53 skilfully predicted from the modelled spring melt pond fraction in May-June calculated with the model
54 developed by Flocco et al. [2010, 2012].

55 Refreezing ponds are difficult to observe because they appear at a time of year when sampling may be
56 challenging. In Figure 1 though, we show one of the few available images of a refreezing pond. This is
57 a snapshot of a video taken in September 2015 during an expedition carried out by Florida University
58 led by David Kadko. The video was taken by William Schmoker, as part of the PolarTREC Program, in
59 the North Canada Basin, north of Barrow, Alaska, by lowering a camera into the ice; it shows a
60 refreezing pond of ~30 cm depth with dendrites of length ~12 cm.



61 While melt ponds enhance sea ice melting rates over summer, they also inhibit basal sea ice formation
62 during their refreezing. When melt ponds refreeze they have two effects on the internal temperature
63 profile of the ice: latent heat release inhibits cooling of the surrounding ice and salt is released in the
64 trapped pond, lowering its freezing temperature. Even once the pond is completely frozen, basal ice
65 growth cannot start until a negative temperature gradient is established at the ice-ocean interface. This
66 second stage often lasts longer than the pond's refreezing itself. The time that it takes for the
67 temperature gradient to allow ice growth to form depends on the internal temperature profile of the ice
68 and the solid fraction of the ice when the pond has refrozen. Flocco et al. [2015] introduced a high
69 resolution, explicit one-dimensional (1D) model of melt pond refreezing that demonstrates that pond
70 refreezing can delay sea ice basal growth by up to a month in areas where refrozen ponds are present.
71 Current GCMs do not include any explicit treatment of melt pond refreezing.

72 In this work we show the impact of the presence of refreezing ponds on the internal sea ice temperature
73 profile and assess the impact of melt pond refreezing on the Autumn growth of Arctic sea ice. We do
74 this by combining results from the 1D refreezing model of Flocco et al. [2015] with pan-Arctic
75 simulations from the widely used Los Alamos National Laboratory sea ice model CICE 5.04 [Hunke et
76 al., 2013]. We determine the volume of artificially high basal sea ice growth at the beginning of winter
77 in current GCMs, where the process of pond refreezing is not accounted for.

78 Section 2 describes the setup of the CICE simulation and our 1D, three-layer refreezing model. Our
79 results are presented and discussed in section 3, with conclusions presented in section 4.

80 **2. Methods**

81 We aim to assess the bias introduced in calculations of Autumn basal sea ice volume growth in GCMs
82 caused by the lack of treatment of refrozen ponds, using the combined results from a recently
83 developed a 1D, three-layer model of refreezing melt ponds [Flocco et al., 2015] and the CICE sea ice
84 model.

85 **2.1 CICE setup**

86 CICE is a dynamic-thermodynamic sea ice model designed for inclusion in a global climate model.
87 Applying the prognostic melt pond model [Flocco et al., 2012] we performed a stand-alone sea-ice
88 simulation for the pan-Arctic region (~40 km grid resolution) over the period 1979 to September 2013



89 using NCEP-DOE-2 Reanalyses data as atmospheric forcing. We implemented a prognostic C-shape
 90 salinity profile for the pond layer to realistically calculate the freezing of ponds [Flocco et al., 2015].
 91 Otherwise, the model used is the CICE version 5.04 [Hunke et al. 2013] and the setup is the same as
 92 was used in Schroeder et al. [2014], using anisotropic rheology, but with 15 instead of 5 ice thickness
 93 categories. The larger number of categories helps reduce large jumps in the ice thickness distribution
 94 and distribution of melt ponds. The applied melt pond scheme only affects the surface albedo and the
 95 freshwater flux into the ocean, otherwise the pond layer is virtual and there is no direct impact on the
 96 temperature profiles in the ice and snow layers.

97 2.2 Melt pond refreezing model

98 The 1D, three-layer model simulates a layer of sea ice covered by a freezing trapped melt pond with an
 99 ice lid on its surface. A schematic of the initial condition of the system is shown in Figure 2.

100 The model determines the sea ice internal temperature T in the lid and in the ice underneath the pond
 101 by solving mushy layers equations in the two ice layers [Flocco et al., 2015]:

$$102 \quad c_{eff} \frac{\partial T}{\partial t} = \frac{\partial}{\partial z} \left(k_{eff} \frac{\partial T}{\partial z} \right) + \frac{\partial F_{net}(z)}{\partial z}, \quad (1)$$

103 where F_{net} is the net radiative flux, c_{eff} is the effective volumetric heat capacity defined by

$$104 \quad c_{eff} = c_i + \frac{T_L(S_{bulk}) - T_L(0)}{\theta^2} L, \quad (2)$$

105 [Bitz and Lipscomb, 1999; Feltham et al., 2006], where $c_i = 1.883 \times 10^6 \text{ J}/(\text{m}^3 \text{ K})$ is the specific
 106 volumetric heat capacity of sea ice, $T_L(S_{bulk})$ denotes the liquidus (freezing) temperature of sea ice with
 107 salinity S_{bulk} (e.g. $T_L(0)=0^\circ\text{C}$), $\theta = T - T_L(0)$, and $L = 3.014 \times 10^8 \text{ J m}^{-3}$ is the volumetric latent heat of
 108 fusion of pure ice [Bailey et al., 2010]. The effective thermal conductivity of sea ice is given by

$$109 \quad k_{eff} = k_{bi} - (k_{bi} - k_b) \frac{T_L(S_{bulk}) - T_L(0)}{\theta}, \quad (3)$$

110 where k_{bi} and k_b are, respectively, the conductivities of bubbly ice and brine, given by

$$111 \quad k_{bi} = \frac{2k_i + k_a - 2V_a(k_i - k_a)}{2k_i + k_a + 2V_a(k_i - k_a)} k_i \quad (4)$$



112 and

$$113 \quad k_b = 0.4184(1.25 + 0.030\theta + 0.00014\theta^2) \quad (5)$$

114 [Schwerdtfeger, 1963], where $k_i = 1.16 (1.91 - 8.66 \times 10^{-3} \theta + 2.97 \times 10^{-5} \theta^2)$ W (m K)⁻¹ is the
115 conductivity of pure ice [Sakazume and Seki, 1978], $k_a = 0.03$ W (m K)⁻¹ is the conductivity of air
116 [Weeks and Ackley, 1986], and we have assumed a constant $V_a = 0.025$ as the fractional volume of air
117 in sea ice [Timco and Frederking, 1996].

118 At the ice lid-air interface the model solves a surface energy balance. A double radiation scheme is
119 applied to the three layers of the model [Taylor and Feltham, 2004] to calculate the radiative fluxes.
120 Continuity of temperature is maintained at the interfaces between the internal layers, which are held at
121 their liquidus temperatures. The temperature at the ice-ocean interface is set to the freezing point of the
122 ocean, which depends on the ocean salinity. The ice growth at the top and at the bottom of the trapped
123 pond is calculated from Stefan conditions at both interfaces.

124 The salinity in the pond is treated semi-analytically and presents maxima in the solutal boundary layers
125 at both ice-pond interfaces where freezing takes place and leads to salt release [Flocco et al., 2015]. A
126 fraction of the salt contained in the refreezing pond is trapped in the growing sea ice layers depending
127 on the sea ice solid fraction at the interface, therefore, in time, the bulk salinity of the lid and of the sea
128 ice at the bottom of the pond evolves. In particular, during every simulation timestep the ice bulk
129 salinity increases creating a gradient in the lid and in the ice underneath the pond.

130 We performed simulations over 60 days of the Autumn refreezing period starting with forcing from the
131 1st of September, with varying pond depths (10 to 60 cm) and sea ice thicknesses (0.5 to 2.1 m), using a
132 daily NCEP-DOE-2 climatology for atmospheric forcing [Kanamitsu et al., 2013]. In order to apply
133 representative forcing fields, 2-m air temperature and incoming long-wave and short-wave radiation
134 fluxes are spatially averaged over the area of the Arctic Ocean which is covered by melt ponds. For
135 calculating the mean forcing fields each grid point is weighted with its melt pond fraction, given by its
136 climatological mean on the 1st of September from our CICE simulation.



137 **3. Results**

138 **3.1 Pond statistics from CICE simulation**

139 Figure 3 shows a climatology of total and trapped melt pond fraction in the Arctic based on our 35 year
140 long CICE simulation. In agreement with previous studies [Flocco et al., 2010, 2012; Schroeder et al.,
141 2014] melt ponds start to form in the second half of May, reach a maximum fraction in mid July (35%
142 coverage) and are mostly covered by an ice lid by the end of August. In the last decade the maximum
143 pond fraction occurs earlier showing that the melting season starts earlier than in the past. Trapped
144 ponds exist in August and September, covering up to 15% of the sea ice area during August but it is
145 worth noticing that the total and the trapped pond fraction show high inter-annual variability. While the
146 maximum total pond fraction is about 10% higher in the later decade than in the 1980s, the trapped
147 pond fraction has decreased. We believe that this decrease is caused by the shift to a predominantly
148 thinner first year ice cover, which tends to become ponded and melt completely rather than retain pond
149 water at its surface.

150 The relative percentages of pond depths on the 1st of September, averaged over 1979-2013, occurring
151 over each of the 15 ice thicknesses used in CICE is shown in figure 4. The pond depth distribution
152 covers the whole range from a few millimetres up to more than 1 m. 31% of all ponds are shallow
153 ponds (thinner than 10 cm) and 1.9% of the ponds are deeper than 1 m. The average pond depth is 26
154 cm, a typical value found in field experiments [Polashenski, et al., 2012].

155 **3.2 Results from the 1D, three-layer model**

156 We use the 1D model of Flocco et al. [2015] to simulate the refreezing of ponds of variable depth over
157 sea ice thicknesses ranging from 0.55 m to 2.10 m (the mean ice thickness in our CICE ice categories
158 3, 5, 6 and 8) for a period of 60 days. As an example, if we consider a sea ice thickness of 1.05 m and a
159 melt pond of 0.3 m, the pond freezes in 19 days (stage I), then in the following 24 days a temperature
160 gradient in the sea ice allowing basal ice growth is established (stage II), and in the remaining 17 days
161 of the simulation basal sea ice growth takes place (stage III).

162 The trapped pond reaches a maximum salinity of 71 psu within the upper solutal boundary layer at the
163 lid interface and 55 psu in its interior due to the rejection of salt into the pond.



164 The minimum melt pond depth that we use as threshold to consider the pond to be refrozen (2 cm), is
165 reached before the pond effectively becomes a brine pocket and starts migrating downwards dissolving
166 the ice at the bottom of the pond (see Flocco et al. [2015] for more details). These results are shown in
167 Figure 5 where it can be observed that in our reference case (ice thickness = 1.05 m and pond depth =
168 30 cm), the ablation of the ice at the bottom of the pond (6 cm) is comparable in magnitude to the basal
169 sea ice growth (7 cm). In Figure 5 we also show the basal ablation at the ice ocean interface, which is a
170 process that occurs at the beginning of each simulation while the pond is still freezing and the pond
171 bottom temperature is above the freezing temperature of the sea water. It is interesting to notice that
172 this process is more important for thinner pond depths: once the whole pond has frozen, the total ice
173 thickness is smaller and the ice growth is faster, therefore the ice basal growth exceeds the basal
174 ablation at the ice-ocean interface. The contrary happens for deeper ponds.

175 If we consider a layer of unponded ice with a starting ice thickness of 1.05 m, we can compare the
176 corresponding sea ice growth with that of the ponded ice of the same thickness. A layer of sea ice 1.05
177 m thick with no pond cover (the “slab case”) would grow by 1.4 cm during stage I, 7.7 cm during stage
178 II, plus a subsequent 11.5 cm during stage III, for a total of 20.6 cm in 60 days. Growth of unponded
179 ice occurs at the base of the ice by freezing sea water with a prescribed salinity of 33 psu, a typical
180 value found in the Arctic. By contrast, ice growth of the ponded ice is mainly due to the pond
181 refreezing. In fact, the total thickness of the ice slab of 1.05 m overlaid by a 30 cm pond has a final
182 thickness of 1.37 m: this figure is the sum of the lid growth, the basal growth and ablation at the bottom
183 of the trapped pond during the pond refreezing.

184 Figure 6 shows the evolution of temperature profile during refreezing for (initially) ponded and
185 unponded sea ice. Refreezing of the trapped pond prevents cooling of the ice beneath the pond, creating
186 a relatively warm layer insulating the ice beneath the pond. Basal ablation at the ocean interface
187 occurring during pond refreezing can overcome the basal growth after the pond has refrozen. In Figure
188 6 we see that during the refreezing of a 30 cm pond, 7 cm of ice at the ocean interface melts, and then,
189 once a negative temperature gradient is established, only 6 cm of ocean water is frozen during the
190 remaining days of the experiment run.

191 By extending our calculations to a range of sea ice thicknesses and melt pond depths, we reach a more
192 extensive set of results presented in Figure 7. Figure 7a shows the basal ice growth for unponded ice



193 and for ponded ice from the 1D model when considering a layer of sea ice of thickness 1.05 m covered
194 by ponds of depths varying from 0.1 to 0.6 m. For increasing pond depths most of the estimated
195 inhibited basal growth occurs in the second stage of pond refreezing, revealing the importance of
196 simulating the evolution of the temperature profile in the refrozen pond and sea ice. Figure 7b shows
197 the inhibited basal ice growth for ponded ice for the same experiment during stage I and stage II: this is
198 the amount of basal sea ice growth in a slab of ice during time equivalent to stage I and stage II.

199 In Figure 7a the difference between the unponded and ponded basal growth is equal to that shown in
200 Figure 7b plus the decreased sea ice basal growth happening in stage III, when basal growth occur in
201 both cases. The same holds for figure 7c and 7d.

202 For simulations with a fixed pond depth of 0.3 m over varying sea ice thickness we see that the
203 inhibiting effect of pond refreezing on basal sea ice growth is a function of the underlying ice thickness
204 (Fig. 7c). The ratio of inhibited growth between Stage I and Stage II depends on the initial ice thickness
205 (Fig. 7d). For sea ice thickness greater than 1.4 m basal growth is not observed within the 60 days of
206 model simulation. This is because it takes longer for the heat to be transferred to the ocean through
207 thicker ice and therefore it takes longer for basal growth to start.

208 *3.3 Combining results from 1D model and CICE*

209 We implemented solutal boundary layers into the melt pond refreezing scheme of Flocco et al. [2012]
210 in the CICE sea ice model. This allows us to determine the inhibited ice growth during the pond
211 refreezing process (Stage I) for our CICE model. We have compared the inhibited basal sea ice growth
212 of the 1D model corresponding to Stage I with our modified CICE model for a range of initial pond and
213 ice thicknesses and the two models present similar results, suggesting that the modifications to CICE
214 are adequate for Stage I (Figure 8). This figure shows a comparison for 4 ice thickness categories
215 (0.55 m, 1.05 m, 1.35 m, 2.1m) and pond depths ranging from 30 to 60 cm. Thinner ponds have been
216 omitted from the comparison because their life time is overestimated in CICE due to the redistribution
217 of melt water from thicker to thinner ice categories.

218 In our comparison we only consider Stage I because CICE does not account for the remaining inhibited
219 growth during Stage II. To combine the results of the two models, we consider again the results shown
220 in figure 7.



221 In order to find the total inhibited growth due to the presence of melt ponds we combine the CICE
222 estimate of the inhibited growth in Stage I with the ratio of inhibited growth in Stage II to Stage I from
223 the 1D model (Figure 7b+d). For example, for a pond depth of 30 cm and sea ice thickness of 1.05 m
224 the ratio between the pond freezing time (Stage I) and the time to reach a sea ice growth temperature
225 gradient (Stage II) is about $\sim 1:5$. The inhibited growth of 1.4 cm during Stage I from the modified
226 CICE model corresponds to an inhibited growth of 7.7 cm during Stage II from the 1D model.

227 Integrating the CICE results for the inhibited growth corresponding to Stage I over the whole Arctic,
228 we derive a 1979-2013 average value of $23 \pm 9 \text{ km}^3$ with a maximum value of 43 km^3 in 1983.
229 Applying the ratio between Stage I and Stage II from our 1D model for each pond depth and ice
230 thickness category individually, we calculate the total inhibited ice growth. Figure 9 shows the time
231 series of inhibited ice growth where we observe a decreasing trend of $-4.4 \text{ km}^3/\text{year}$ with considerable
232 interannual variability. The trend arises because the ice cover has thinned and thus the required
233 temperature profile in the ice for refreezing is more quickly established. The thinner ice is also more
234 likely to melt completely.

235 Over 1979-2013 the mean inhibited ice growth is $126 \pm 55 \text{ km}^3$ with a maximum value of 228 km^3 in
236 1983. In Figure 10 we show the magnitude of the local inhibited basal ice growth for the extreme year
237 1983. In this map the grid cell averaged inhibited ice growth is above 10 cm for large areas in the
238 Canadian Arctic and can reach values as high as 20 cm.

239 4. Conclusion

240 The presence of refreezing melt ponds delays basal sea ice growth in Autumn: ice only thickens after
241 (1) the pond water has been fully frozen and (2) a temperature gradient within the ice has been
242 established that will conduct heat from the ocean to the atmosphere. In addition, melt ponds cause basal
243 melt because the pond bottom temperature is above the sea water freezing temperature. These
244 processes have not been accounted for so far in any climate model. A stand-alone simulation with a
245 version of the Los Alamos National Laboratory CICE sea ice model shows an overestimated basal sea
246 ice growth of around 20 km^3 due to not considering the first process (pond refreezing). The impact of
247 the second process cannot be determined from CICE, however, using the pond depth distribution from
248 CICE, simulations with a 1D melt pond refreezing model show that the impact on refreezing of the



249 second stage (establishing the temperature gradient) is generally stronger, leading to a total
250 overestimation of basal ice growth of about 126 km³ on average and up to 228 km³ for individual years
251 in Autumn over the Arctic basin. These values range from 12% to 23% of the amount of sea ice growth
252 estimated from PIOMAS in the same period (September-October) [Zhang et al., 2003].

253 The total ice mass balance is not too strongly affected by neglecting the refreezing process. Our CICE
254 simulations show that pond refreezing contributes 113 km³ of ice, which is similar to the mean
255 overestimation of basal ice growth of 128 km³. However, the source of ice volume increase in Autumn
256 is of relevance to related processes: our results suggest existing estimates of negative buoyancy
257 production at the ice—ocean interface due to salt release during sea ice growth have been
258 overestimated in models.

259 There is a decreasing volume of refreezing ponds during the last decade, primarily due to the shift from
260 a permanent to a more seasonal Arctic sea ice cover. The majority of ponds are present on thin ice,
261 which are more likely to disappear at the end of summer. While the overestimation of basal ice growth
262 by ignoring pond refreezing has decreased in the last few decades, the overestimated basal growth is
263 not negligible.

264

265 **Acknowledgments**

266

267 We would like to acknowledge the Natural Environmental Research Council for supporting this work.

268 The CICE model with the supportive documentation can be found at
269 <http://oceans11.lanl.gov/drupal/CICE>. The NCEP data are available for download at
270 www.esrl.noaa.gov/psd/data/gridded/data.ncep_reanalysis2.html.

271



- 272 **5. References**
- 273 Bailey, E., D. L. Feltham, and P. R. Sammonds (2010), A model for the consolidation of rafted sea ice,
274 J. Geophys. Res., 115, C04015, doi:10.1029/2008JC005103.
- 275 Bitz, C., and W. Lipscomb (1999), An energy-conserving thermodynamic model of sea ice, J.
276 Geophys. Res., 104, 15,669–15,677, doi:10.1029/1999JC900100.
- 277 Feltham, D. L., Untersteiner, N., Wettlaufer, J. S. and Worster, M. G. (2006) Sea ice is a mushy layer.
278 Geophysical Research Letters, 33 (14). L14501. ISSN 0094-8276 doi: 10.1029/2006GL026290.
- 279 Flocco, D., D. L. Feltham, and A. K. Turner (2010), Incorporation of a physically based melt pond
280 scheme into the sea ice component of a climate model, J. Geophys. Res., 115, C08012,
281 doi:10.1029/2009JC005568.
- 282 Flocco, D., D. Schroeder, D. L. Feltham, and E. C. Hunke (2012), Impact of melt ponds on Arctic sea
283 ice simulations from 1990 to 2007, J. Geophys. Res., doi:10.1029/2012JC008195.
- 284 Flocco, D., D. L. Feltham, E. Bailey, and D. Schroeder (2015), The refreezing of melt ponds on Arctic
285 sea ice, J. Geophys. Res. Oceans, 120, 647–659).
- 286 Hunke, E. C., W. H. Lipscomb, A. K. Turner, N. Jeffery, and S. Elliott (2013), CICE: the Los Alamos
287 Sea Ice Model Documentation and Software User’s Manual Version 5.0.
- 288 Kanamitsu, M., W. Ebisuzaki, J. Woollen, S-K Yang, J.J. Hnilo, M. Fiorino, and G. L. Potter, NCEP-
289 DOE AMIP-II Reanalysis (R-2): 1631-1643, Bulletin of the American Meteorological Society,
290 (2002, updated 2013).
- 291 Laxon, S., N. Peacock, and D. Smith (2003), High interannual variability of sea ice thickness in the
292 Arctic region, Nature, 425 (6961), 947–950.
- 293 Perovich D. K., Richter-Menge J. A., (2009) Loss of Sea Ice in the Arctic, Annual Review of Marine
294 Science, Vol. 1: 417 – 441.
- 295 Perovich, D. K., J. A. Richter-Menge, K. F. Jones, and B. Light (2008), Sunlight, water, and ice:
296 Extreme Arctic sea ice melt during the summer of 2007, Geophys. Res. Lett., 35, L11501,
297 doi:10.1029/2008GL034007.



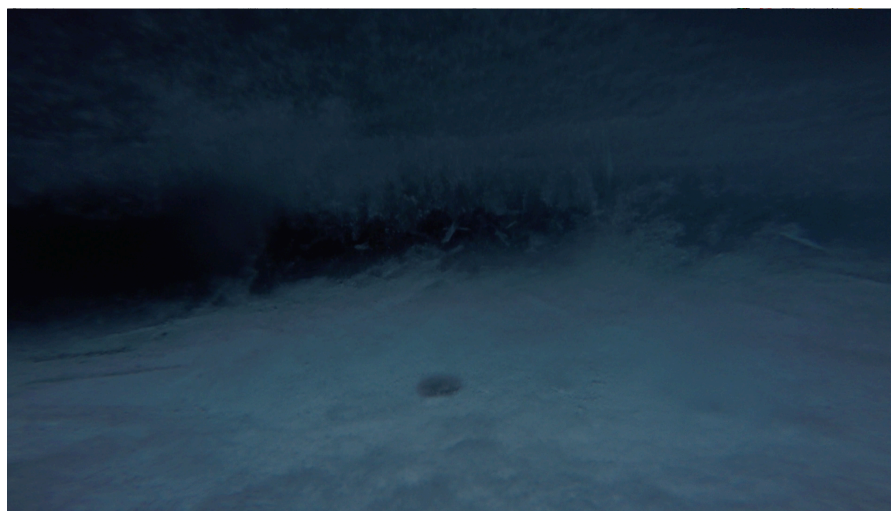
- 298 Perovich, D.K., W.B. Tucker III, and K.A. Ligett (2002), Aerial observations of the *evolution of ice*
299 *surface conditions during summer*, *J. Geophys. Res.*, *107 (C10)*, 8048,
300 doi:10.1029/2000JC000449.
- 301 Polashenski, C., D. Perovich, and Z. Courville (2012), The mechanisms of sea ice melt pond formation
302 and evolution, *J. Geophys. Res.*, *117*, C01001, doi:10.1029/2011JC007231.
- 303 Sakazume, S., and N. Seki (1978), Thermal properties of ice and snow at low temperature region, *Bull.*
304 *JSME*, *44(382)*, 2059–2069.
- 305 Schröder D., D. L. Feltham, D. Flocco, M. Tsamados, (2014), September Arctic sea-ice minimum
306 predicted by spring melt-pond fraction. *Nature Clim. Change*, DOI: 10.1038/NCLIMATE2203.
- 307 Schwerdtfeger, P. (1963), The thermal properties of sea ice, *J. Glaciol.*, *4(36)*, 789–807. Sakazume, S.,
308 and N. Seki (1978), Thermal properties of ice and snow at low temperature region, *Bull. JSME*,
309 *44(382)*, 2059–2069.
- 310 Stroeve, J. C., T. Markus, L. Boisvert, J. Miller, and A. Barrett (2014), Changes in Arctic melt season
311 and implications for sea ice loss, *Geophys. Res. Lett.*, *41*, 1216–1225,
312 doi:10.1002/2013GL058951.
- 313 Taylor, P. D., and D. L. Feltham (2004), A model of melt pond evolution on sea ice, *J. Geophys. Res.*,
314 *109*, C12007, doi:10.1029/2004JC002361.
- 315 Timco, G. W., and R. M. W. Frederking (1996), A review of sea ice density, *Cold Reg. Sci. Technol.*,
316 *24*, 1–6, doi: 10.1016/0165-232X(95)00007-X.
- 317 Tsamados M., Feltham, D. Petty, A., Flocco, (2015), Processes controlling surface, bottom and lateral
318 melt of Arctic sea ice in a state of the art sea ice model, *Phil. Trans. R. Soc. A* *2015* 373
319 20140167; DOI: 10.1098/rsta.2014.0167.
- 320 Weeks, W. F., and S. F. Ackley (1986), The growth, structure and properties of sea ice, in *The*
321 *Geophysics of Sea Ice*, NATO ASI Ser., Ser. B., vol. 146, edited by N. Untersteiner, pp. 9–164,
322 Martinus Nijhoff, Dordrecht, Netherlands



323 Zhang, J and D.A. Rothrock, (2003) Modeling global sea ice with a thickness and enthalpy distribution
324 model in generalized curvilinear coordinates, Mon. Wea. Rev. 131(5), 681-697 (updated 2012).
325



326 **Figure 1**



327

328 **Figure 1: Refreezing pond from field observation (Bill Schmoker, PolarTREC 2015, Courtesy of**
329 **Arctic Research Consortium of the United States.).**

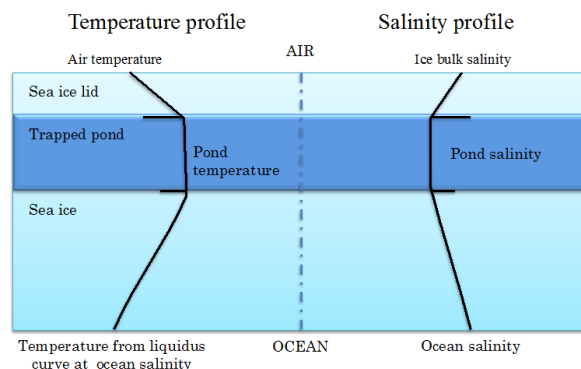
330

331

332



333 **Figure 2**



334

335 **Figure 2: Configuration of the phases in the one-dimensional, three-layer model: the left panel**
336 **shows the temperature profile in the three layers: ice lid, pond and sea ice. The right panel**
337 **shows the salinity profile in the three layers. The temperature minima at the pond interfaces are due to**
338 **the high salinity at the upper and lower boundary layers due to salt rejection from ice formation.**

339

340

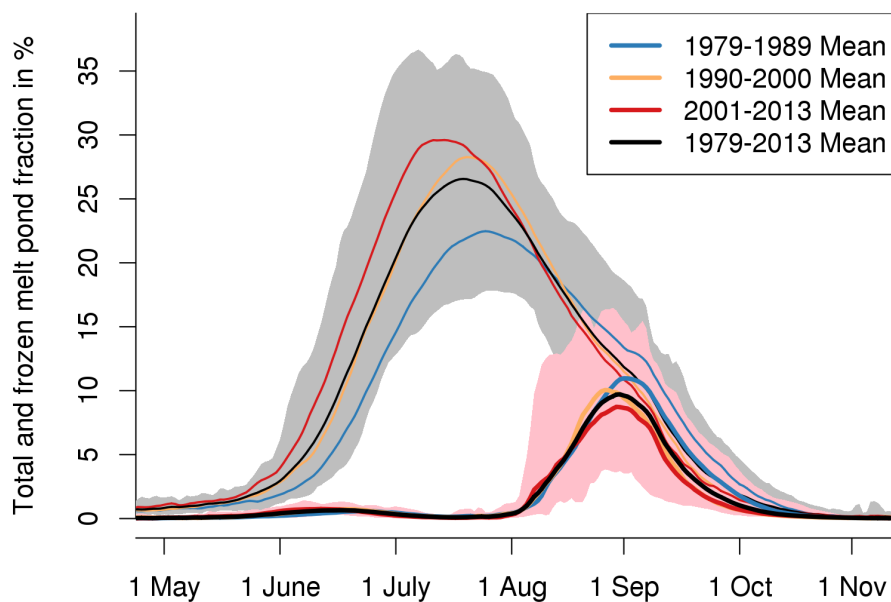
341

342



343 **Figure 3**

344



345

346 **Figure 3: Total and frozen melt pond surface fractions in % (respectively the grey and the pink**
347 **areas). The average values for the decades from 1979 to 2013 are superimposed over the pond**
348 **area and the refrozen pond area.**

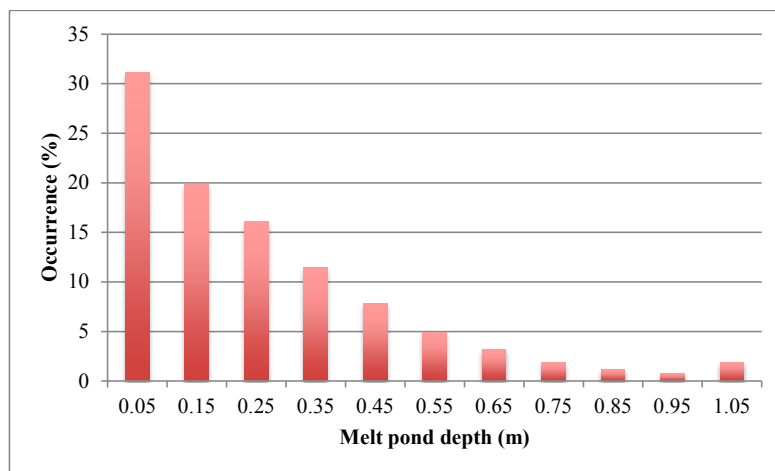
349

350

351



352 **Figure 4**



353

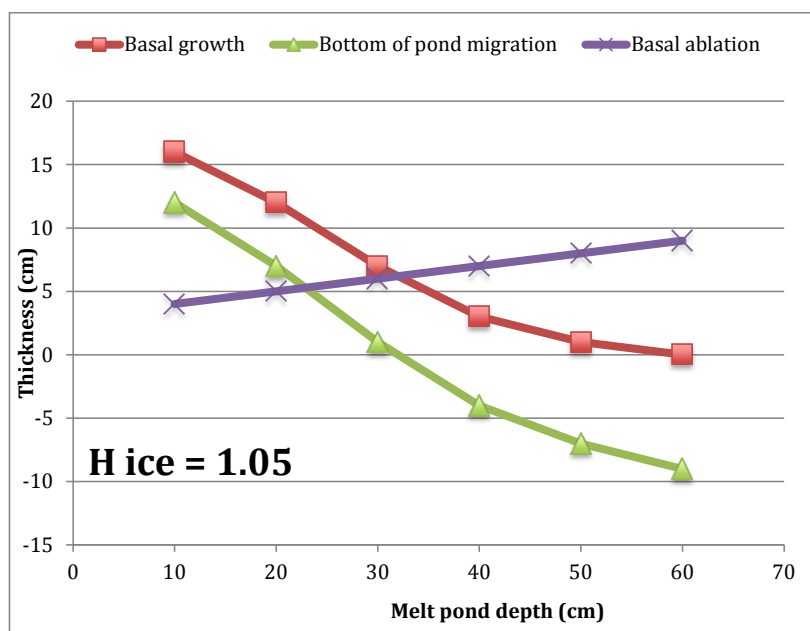
354 **Figure 4: Arctic basin-wide distribution of pond depth on 1st September (average of 1979-2013)**
355 **over all ice thickness categories for the CICE model.**

356

357



358 **Figure 5**
359



360
361
362
363
364
365
366
367
368
369
370
371

Figure 5: Bottom of the pond ablation, basal ice growth and basal ablation at the ocean interface at the end of the 60 days simulation beginning on 1st September for an initial ice thickness of 1.05 m and a range of melt pond depths.



372 **Figure 6**
373

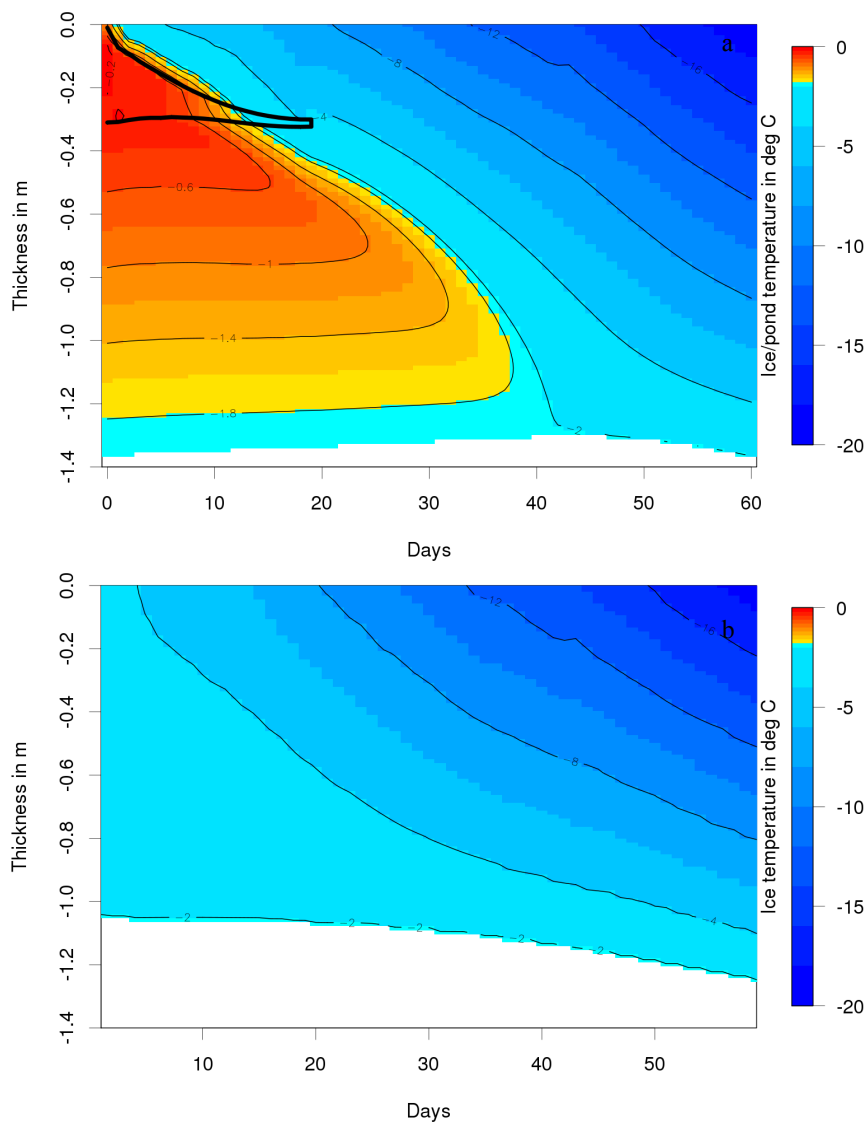


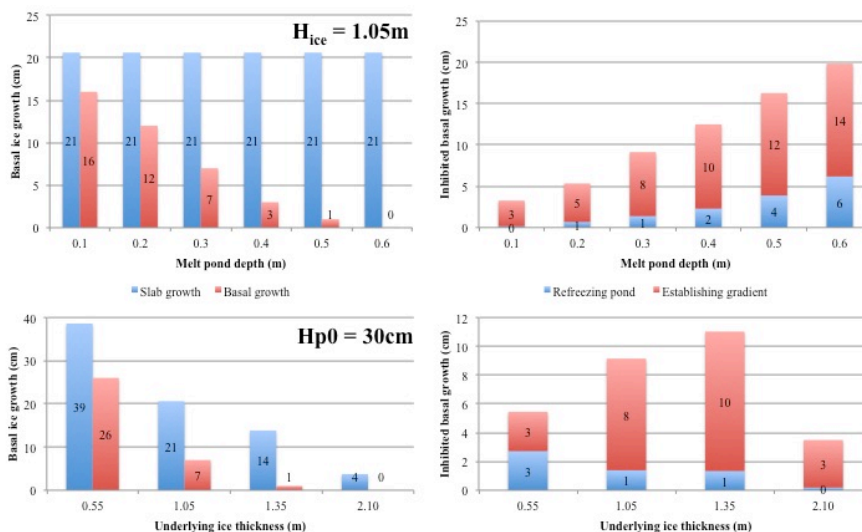
Figure 6: (a) Sea ice internal temperature profile for a refreezing pond of 30 cm over an ice layer of 1.05 m. The bold black lines denote the phase boundaries at the top and bottom of the trapped pond. (b) Sea ice internal temperature profile ice layer of 1.05 m

374
375



376 **Figure 7**

377



378

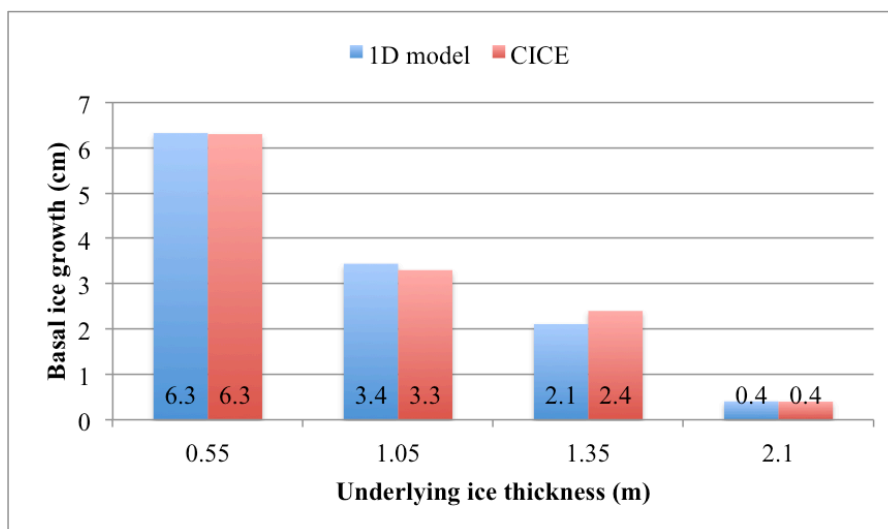
379

380 **Figure 7 (a, b) Basal sea ice growth and inhibited basal growth for the refreezing pond model in**
 381 **comparison with a slab model that grows by 21 cm over 60 days for varying pond depths; (c, d)**
 382 **Basal sea ice growth and inhibited basal growth for the refreezing pond model with a 0.3 m pond**
 383 **over a 1.05 m ice slab in comparison with a slab model over 60 days for varying ice thicknesses.**
 384 **See text for description.**

385



386 **Figure 8**



387

388

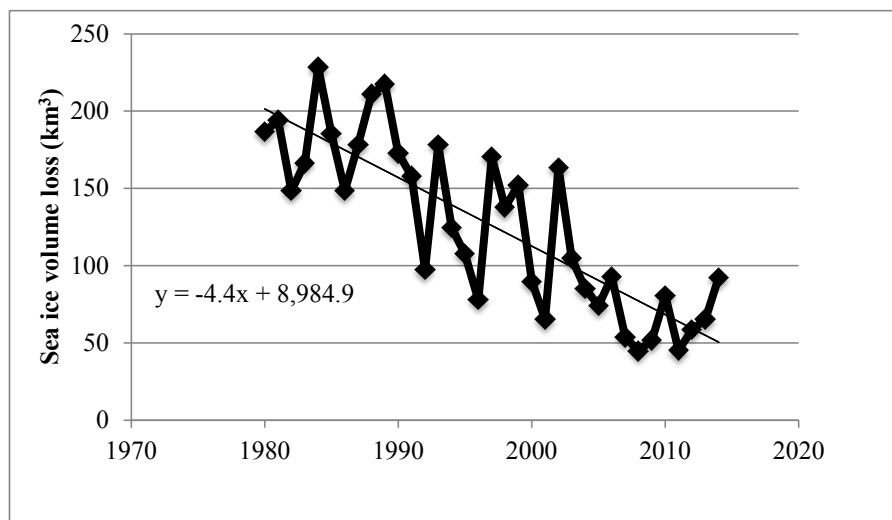
389 **Figure 8: Comparison of inhibited basal ice growth during pond refreezing (Stage I) in the 1D**
390 **model and in CICE: this is the basal growth that would occur in the absence of a refreezing pond.**
391 **This histogram uses the averaged value of ice growth in the 1D, three layer model averaged over**
392 **a range of pond depths of 30-60 cm.**

393



394 **Figure 9**

395



396

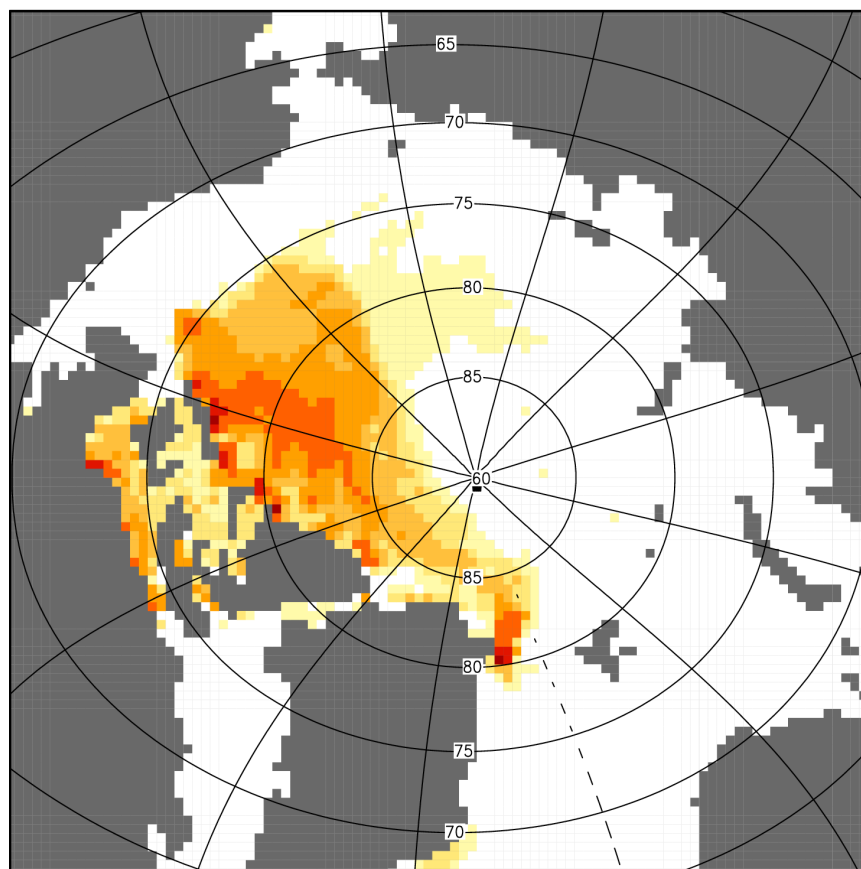
397

398 **Figure 9: Time series of total inhibited growth from 1979 to 2013.**

399



400 **Figure 10**



Total inhibited ice growth in cm



401

402 **Figure 10: Total inhibited sea ice growth volume in 1983 for both Stage I (refreezing of pond, as**
403 **simulated in CICE), and Stage II (establishing of temperature profile for growing of ice, as**
404 **calculated using relationship between growth during Stages I and II for individual pond depths**
405 **and ice thickness categories). The spatially integrated inhibited growth amounts to 228 km³ of sea**
406 **ice.**

407

408

409



410 **Figures captions**

411 Figure 1: Refreezing pond from field observation (Bill Schmoker, PolarTREC 2015, Courtesy of Arctic
412 Research Consortium of the United States.).

413 Figure 2: Configuration of the phases in the one-dimensional, three-layer model: the left panel shows
414 the temperature profile in the three layers: ice lid, pond and sea ice. The right panel shows
415 the salinity profile in the three layers. The temperature minima at the pond interfaces are
416 due to the high salinity at the upper and lower boundary layers due to salt rejection from
417 ice formation.

418 Figure 3: Total and frozen melt pond surface fractions in % (respectively the grey and the pink areas).
419 The average values for the decades from 1979 to 2013 are superimposed over the pond
420 area and the refrozen pond area.

421 Figure 4: Arctic basin-wide distribution of pond depth on 1st September (average of 1979-2013) over all
422 ice thickness categories for the CICE model.

423 Figure 5: Bottom of the pond ablation, basal ice growth and basal ablation at the ocean interface at the
424 end of the 60 days simulation beginning on 1st September for an initial ice thickness of
425 1.05 m and a range of melt pond depths.

426 Figure 6: (a) Sea ice internal temperature profile for a refreezing pond of 30 cm over an ice layer of
427 1.05 m. The bold black lines denote the phase boundaries at the top and bottom of the
428 trapped pond. (b) Sea ice internal temperature profile ice layer of 1.05 m

429 Figure 7: (a, b) Basal sea ice growth and inhibited basal growth for the refreezing pond model in
430 comparison with a slab model that grows by 21 cm over 60 days for varying pond depths;
431 (c, d) Basal sea ice growth and inhibited basal growth for the refreezing pond model with a
432 0.3 m pond over a 1.05 m ice slab in comparison with a slab model over 60 days for
433 varying ice thicknesses. See text for description.

434 Figure 8: Comparison of inhibited basal ice growth during pond refreezing (Stage I) in the 1D model
435 and in CICE: this is the basal growth that would occur in the absence of a refreezing pond.



436 This histogram uses the averaged value of ice growth in the 1D, three layer model
437 averaged over a range of pond depths of 30-60 cm.

438 Figure 9: Time series of total inhibited growth from 1979 to 2013.

439 Figure 10: Total inhibited sea ice growth volume in 1983 for both Stage I (refreezing of pond, as
440 simulated in CICE) and Stage II (establishing of temperature profile for growing of ice, as
441 calculated using relationship between growth during Stages I and II for individual pond
442 depths and ice thickness categories). The spatially integrated inhibited growth amounts to
443 228 km³ of sea ice.